Supplementary Information for:

Structural and Torsional Properties of the RAD51-dsDNA Nucleoprotein Filament

Mina Lee[†], Jan Lipfert[†], Humberto Sanchez[‡], Claire Wyman[‡], and Nynke H. Dekker[*,†]

[†]Department of Bionanoscience, Kavli Institute of Nanoscience, Delft University of Technology, Lorentzweg 1, 2628 CJ Delft, [‡] Department of Genetics, Department of Radiation Oncology, Erasmus University Medical Center, P. O. Box 2040, 3000 CA Rotterdam, The Netherlands.

* To whom all correspondence should be addressed. E-mail: N.H.Dekker@tudelft.nl.

Table of Contents

Supplementary Figure 1. Rotational Fluctuations of a 7.9 kbp dsDNA Monitored in FOMT

Supplementary Figure 2. Force Extension Curves of DNA Before and After Assembly

Supplementary Figure 3. RAD51 Assembly Monitored in FOMT at Saturating Concentrations of RAD51

Supplementary Figure 4. RAD51 Assembly Monitored in FOMT at Subsaturating Concentration of RAD51

Supplementary Figure 5. RAD51 Assembly Monitored in FOMT in the Presence of Mg^{2+}-ATP

Supplementary Figure 6. Comparison of Marker Bead Tracking and Simple XY Tracking for Measurement of RAD51-dsDNA Torsional Response

Supplementary Figure 7. Torque Curves of the RAD51-dsDNA Filament Assembled in Ca^{2+}-ATP

Supplementary Figure 8. Torque Curves of the RAD51-dsDNA Filament Assembled in Ca^{2+}-AMPPNP

Supplementary Figure 9. Torque Curves of the RAD51-dsDNA Filament Assembled in Mg^{2+}-AMPPNP

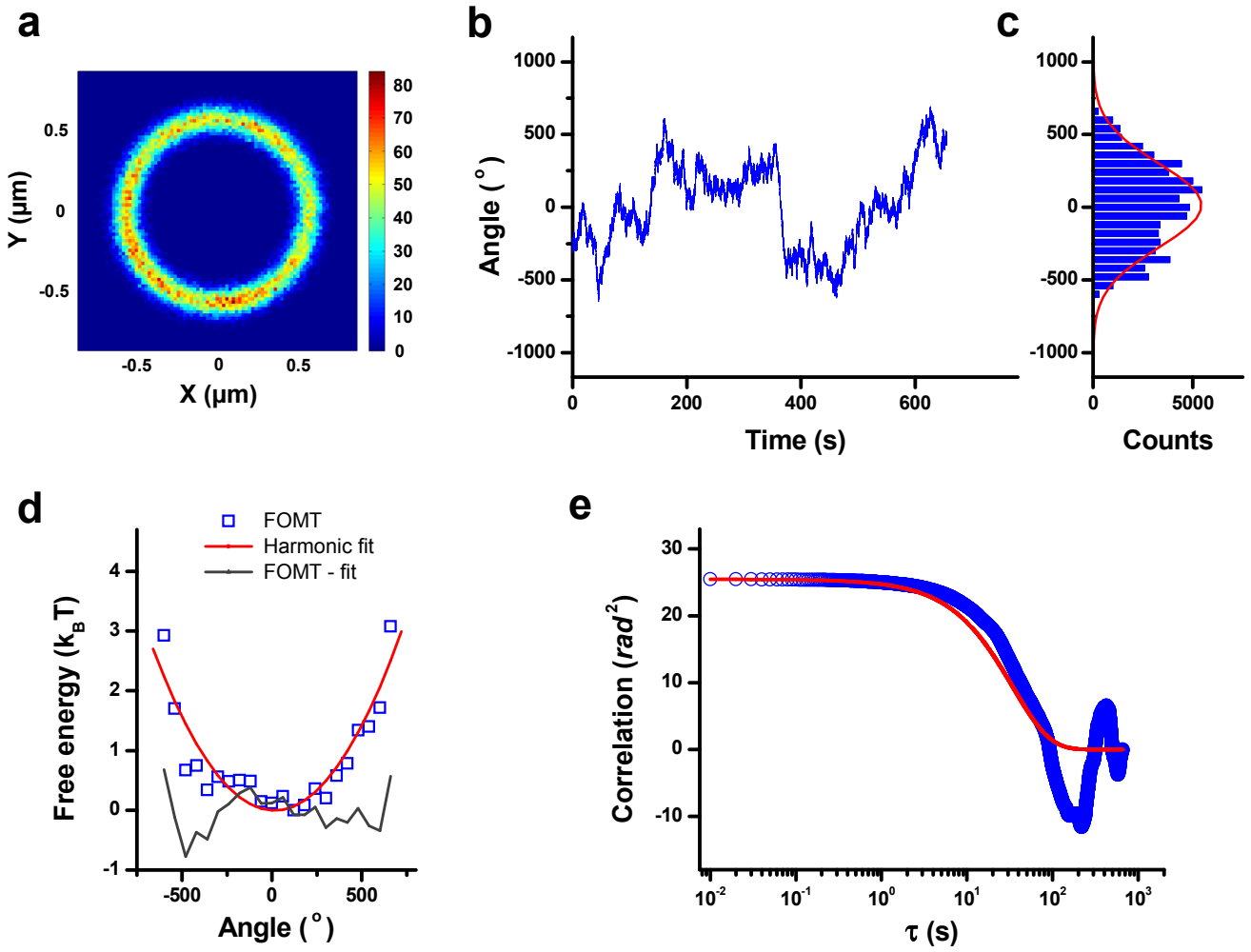

Supplementary Figure 1. Rotational fluctuations of a 7.9 kbp dsDNA Monitored in the FOMT. Data in panels **a**)-**d**) were obtained using a MyOne bead (1.0 µm diameter) attached to a 7.9 kbp dsDNA tether in the FOMT geometry at F = 3.5 pN. **a)** Histogram of the (x, y)-fluctuations. **b)** Rotational fluctuation of the bead determined from the (x, y)-position. **c)** Histogram of the rotational fluctuations. The solid red line is a Gaussian fit with σ_θ = 289°. **d)** The energy landscape implied by the rotational fluctuation density from **b)**. The difference (solid dark grey line) between the landscape implied by the rotational fluctuations (blue squares) and the harmonic approximation (solid red line) with $k_\theta = k_B T/\sigma_\theta^2$ = 0.16 pN·nm/rad is smaller than the thermal energy $k_B T$. Since the magnet has a negligible effect on the rotational fluctuations, the width of the rotational fluctuation is determined by the tether stiffness alone. The width of the fluctuations observed in this experiments corresponds to a torsional persistence length of the tether (26) equal to $C = L_C / \sigma_\theta^2$ = 105 nm, in agreement, within experimental error, with previous measurements of the torsional stiffness of dsDNA (24, 26). **e)** Temporal autocorrelation of the rotational fluctuations. The solid red line is an exponential fit to the data from which we extract the trap stiffness k_θ = 0.16 pN·nm/rad and the friction coefficient γ = 5.4 pN·nm·s implying a characteristic time $\tau_C = \gamma/k_\theta$ = 34 s.

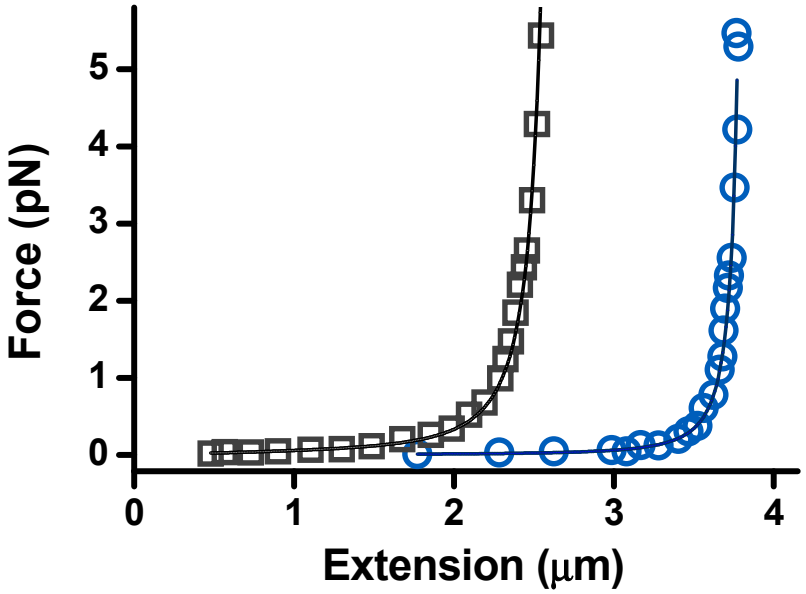

Supplementary Figure 2. Force-extension Curves of DNA Before and After Assembly of RAD51 Filaments. Magnetic tweezers measurements of the force-extension behavior of a 7.9 kbp dsDNA (dark grey squares) and a dsDNA-RAD51 nucleoprotein filament (blue circles) of which the assembly was monitored in the FOMT. The RAD51 filament was assembled at saturating conditions ([RAD51] = 200 nM and F = 3.5 pN) in the presence of Ca^{2+}-ATP. Buffer conditions are described in detail in the Materials and Methods. Bare DNA and RAD51-DNA filaments were torsionally relaxed before the measurements by checking rotation extension curves. Fits of the WLC model yield contour length L_c = 2.7 ± 0.1 μm and bending persistence length L_p = 46 ± 1 nm for bare DNA (solid black line) and L_c = 4.0 ± 0.1 μm and L_p = 241 ± 72 nm for the RAD51 filament (solid navy line). The fitted contour and persistence lengths for DNA are in good agreement with the expected crystallographic length and previously determined values, respectively. The contour length of RAD51 filament is increased by a factor of 1.5-fold after complete assembly compared to bare DNA as expected from EM structural results (10, 14) and single molecule stretching experiments (19, 20). The fitted persistence length of the RAD51 filament of L_p = 241 ± 72 nm is in agreement, within experimental error, with earlier stretching experiments (19, 20).

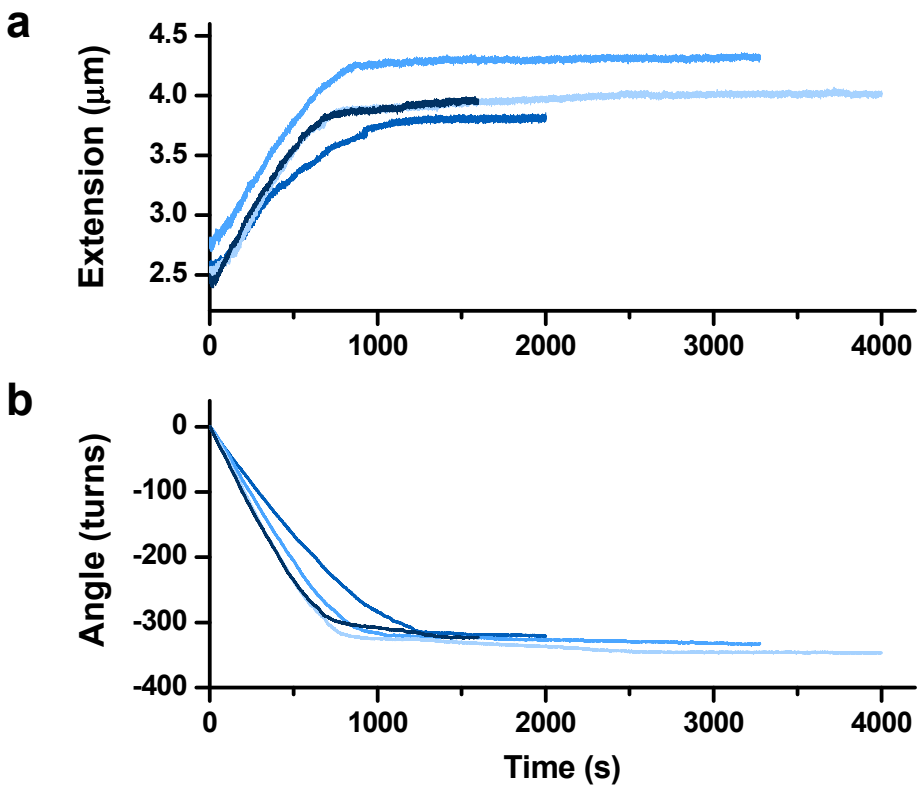

Supplementary Figure 3. RAD51 Assembly Monitored in the FOMT at Saturating Concentrations of RAD51. 4 different assembly traces of RAD51 (from dark blue to light blue) onto 7.9 kbp dsDNA at F = 6 pN and [RAD51] = 400 nM in the presence of Ca^{2+}-ATP. Time traces of **a)** the height z and **b)** the rotation angle of the tethered MyOne beads (1.0 µm diameter). The same color codes were used in **a)** and **b)**.

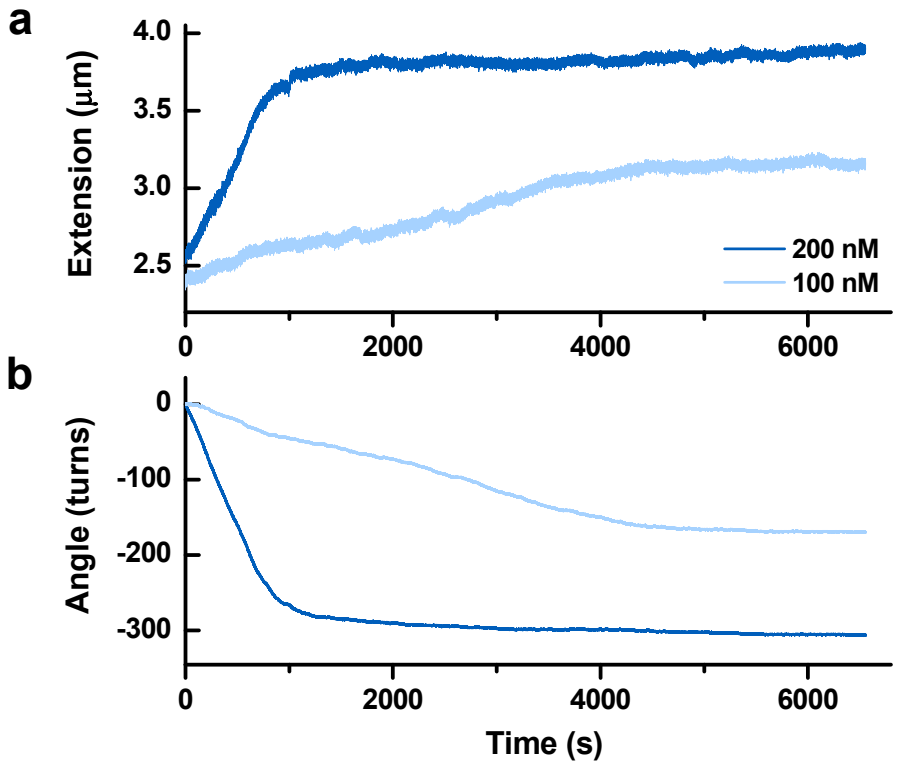

Supplementary Figure 4. RAD51 Assembly Monitored in FOMT at Subsaturating Concentrations of RAD51. An assembly trace of RAD51 onto 7.9 kbp DNA at F = 3.5 pN and [RAD51] = 100 nM (light blue) in the presence of Ca^{2+}-ATP. The trace at 200 nM (dark blue) is shown for comparison. Time traces of **a)** the height z and **b)** the rotation angle of the MyOne bead. The same color codes were used in **a)** and **b)**. At [RAD51] = 100 nM, the assembly was slower compared to that at 200 nM. Furthermore, as the contour length only increased from 2.6 μm to 3.2 μm and total unwinding angle was limited to −170 turns (corresponding to ~47% of full coverage), assembly was incomplete at this lower concentration. Nonetheless, the unwinding angle per RAD51, 50 ± 8° (deduced using the same method as in the main text), remained in agreement with measurements under saturating conditions. The increased error in the unwinding angle per RAD51 results from the uncertainty in determining the contour length of a partially-covered RAD51 filament, which is not as reliable as with fully-covered filaments.

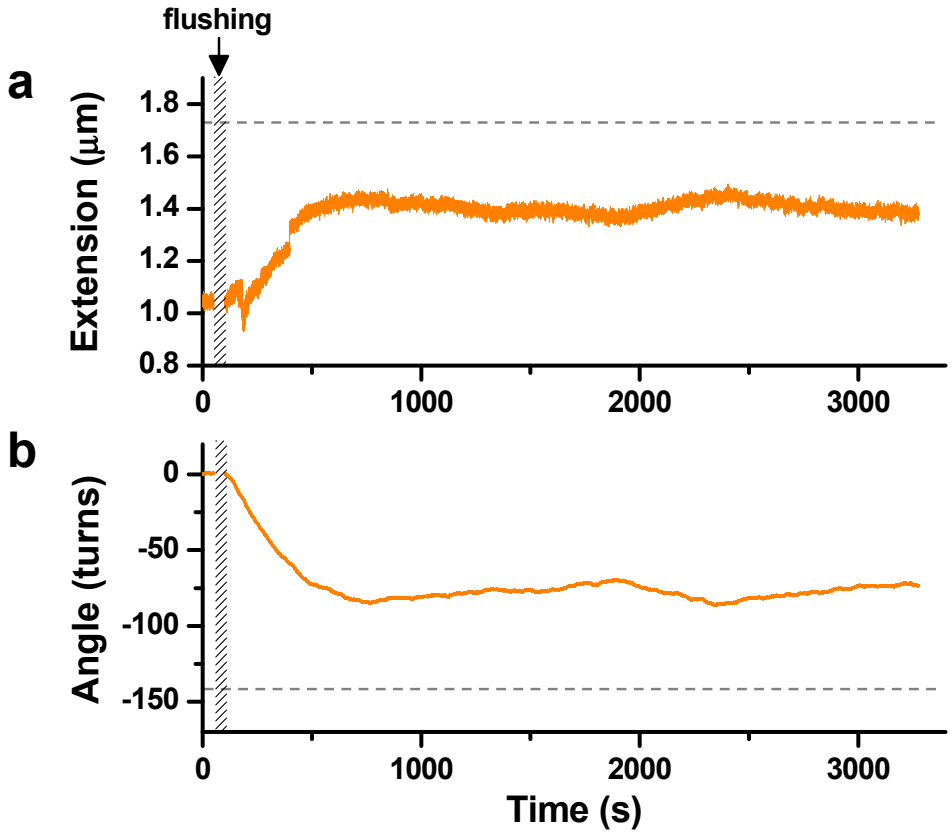

Supplementary Figure 5. RAD51 Assembly Monitored in FOMT in the Presence of Mg^{2+}-ATP. An assembly trace of RAD51 onto 3.4 kbp dsDNA at F = 2.2 pN and [RAD51] = 400 nM in the presence of Mg^{2+}-ATP. The buffer was the same as the Ca^{2+}-ATP buffer, except $MgCl_2$ was added instead of $CaCl_2$. Time traces of **a)** the height z and **b)** the rotation angle of the MyOne bead. Dashed lines in **a)** and **b)** correspond to those expected for full coverage of the DNA by RAD51. We attribute the small abrupt discontinuities in the extension trace of **a)** at 200 and 400 s to nonspecific adhesion of a small portion of the bead-tether complex to the surface followed by subsequent detachment. The unwinding angle per RAD51, 49 ± 8° (deduced using the same method as in the main text), was in agreement with measurements under saturating conditions. The increased error in the unwinding angle per RAD51in this experiment results from the dynamic nature of the assembly in which neither the filament extension nor the bead's angular position reached a steady state.

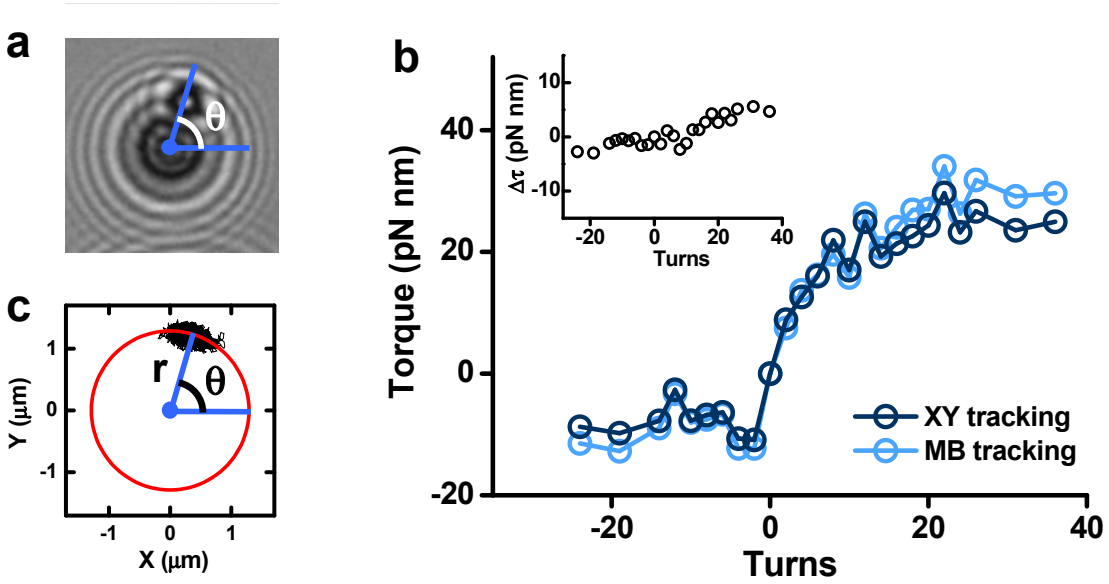

Supplementary Figure 6. Comparison of Marker Bead Tracking and Simple XY Tracking for Measurement of RAD51-dsDNA Torsional Response. a) Defocused CCD image of an M270 bead together with a marker bead (1 μm diameter) used for angular tracking. The attachment procedure of the marker beads and the angle tracking methods are described in the Materials and Methods. The position of the marker bead was tracked using the algorithm previously reported (24, 42). **b)** To compare the tracking methods, a torque measurement on a RAD51-dsDNA filament was performed using both approaches, marker bead tracking (light blue points) and simple (*x*, *y*) tracking (dark blue points), simultaneously. The curves from two methods agreed within the experiment error of ± 3 pN·nm. The inset is the difference between the two tracking methods. **c)** The (*x*, *y*) positions of the main bead shown in **a)**. The red line is the circle fitted to the traces of the bead's free rotation measured in a separate experiment. We have previously shown that the angles determined from the position of the marker bead and the (*x*, *y*) position of the main bead on the circle are tightly coupled (26). Therefore, a circular arc sampled by a bead in the MTT can consequently be converted from Cartesian to polar coordinates.

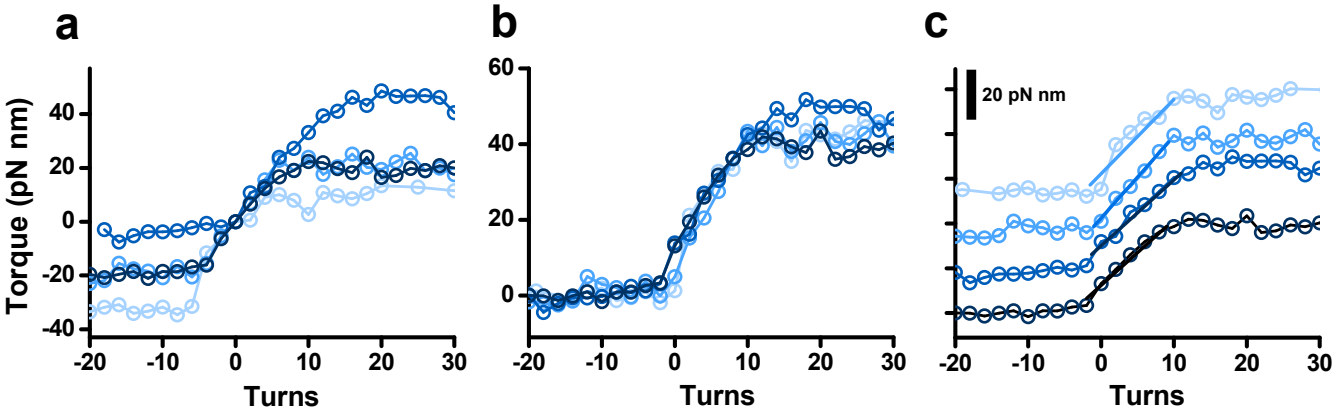

Supplementary Figure 7. Torque Curves of the Filaments Assembled with Ca^{2+}-ATP. a) Four different torque versus applied turns curves (from light blue to dark blue) of RAD51-dsDNA filaments (L_c = 4.1 ± 0.1 μm) assembled in the presence of Ca^{2+}-ATP. All the measurements were performed at F = 3.5 pN and k_θ ~ 300 pN·nm using M270 beads. The buffer conditions are described in the Materials and Methods. Applied turns were numbered with respect to the rotational offset at which the filament was torsionally relaxed so that the extension was maximal. The curves are shifted each other as a result of the uncertainty in the accurate determination of the rotational offset (± 2 turns) which yields an uncertainty in the absolute torque values of ± 8 pN·nm. **b)** To facilitate comparison between the measurements, the torque plateaus upon under-winding and the onset of the linear regime were aligned for all curves. This shows that the shapes of the torque curves are very reproducible. The values of the torque plateaus at negative and positive turns are −20 ± 13 and 24 ± 14 pN·nm, respectively. The difference in torque between the two plateaus is 43 ± 4 pN·nm, with a much reduced SEM. **c)** Stacked representation of the torque versus applied turns curves obtained by displacing the curves in **b)** in y-axis one-by-one to see the reproducibility of the slopes in the linear response regime. The torsional persistence length (C) is determined by linear fits in this regime (solid lines) and equals 504 ± 57 nm (mean and SEM for 4 measurements).

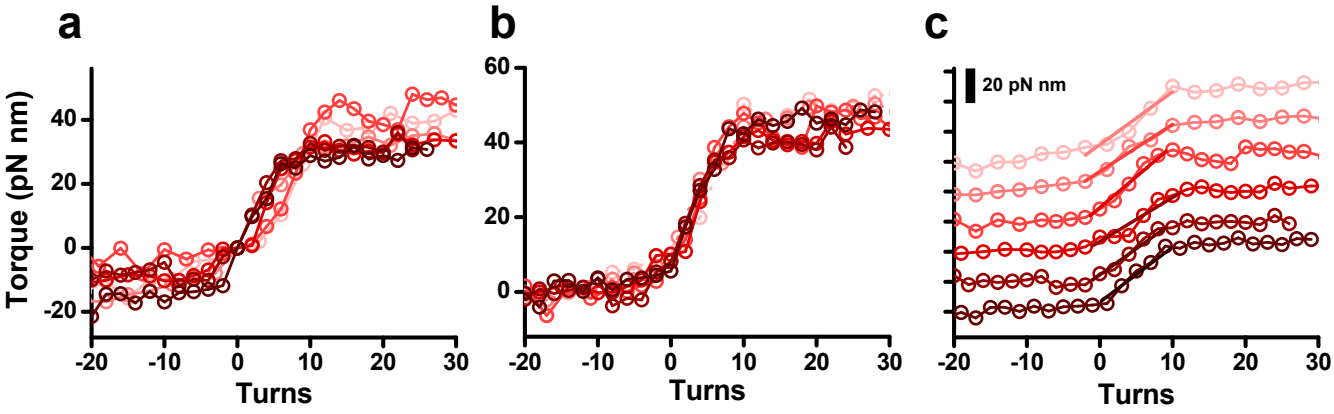

Supplementary Figure 8. Torque Curves of the Filaments Assembled with Ca^{2+}-AMPPNP. a) Six different torque versus applied turns curves (from light red to dark red) of RAD51-dsDNA filaments (L_c = 4.0 ± 0.1 µm) assembled in the presence of Ca^{2+}-AMPPNP. All measurement conditions besides the buffer composition were identical to those described in Supplementary Figure 7. The curves in **b)** and **c)** were generated in the same way as in Supplementary Figure 7b,c to see the reproducibility in torque plateaus and the slopes of the curves. The values of the torque plateaus at negative and positive turns are −10 ± 4 and 35 ± 5 pN·nm, respectively. The difference in torque between the two plateaus is 46 ± 3 pN·nm. The torsional persistence length (*C*) The torsional persistence length (*C*) is determined by linear fits in this regime (solid lines) and equals 540 ± 50 nm (mean and SEM for 6 measurements).

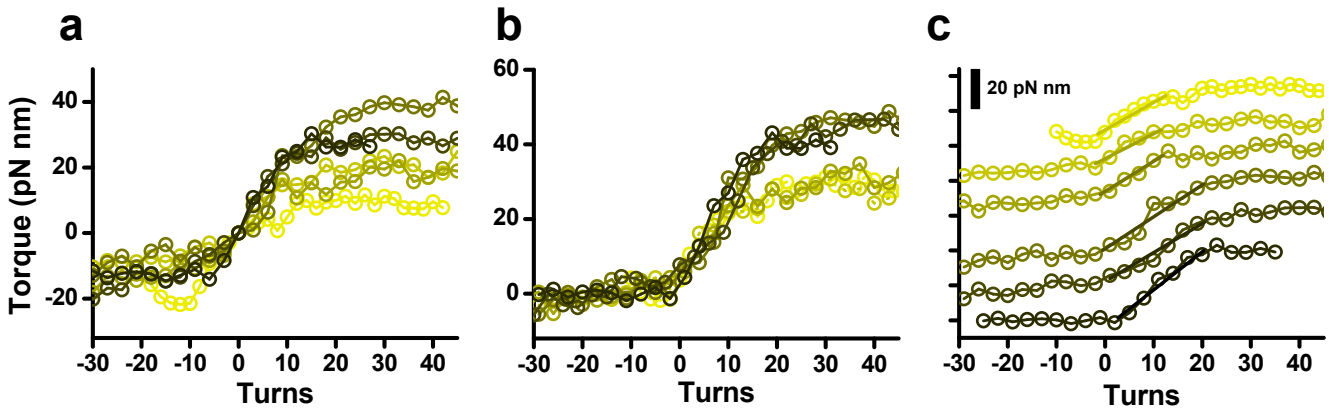

Supplementary Figure 9. Twist Curves of the Filaments Assembled with Mg^{2+}-AMPPNP. a) Six different torque versus applied turns curves (from light yellow to dark yellow) of RAD51-dsDNA filaments (L_c = 4.0 ± 0.1 μm) assembled in the presence of Mg^{2+}-AMPPNP. To directly compare the properties of RecA and RAD51 in similar buffer conditions, three datasets (represented by the lighter yellow curves) were obtained in a buffer at pH 6.2, which is very similar to that used in previous RecA measurement (24). Even though this reduced pH was less optimal for RAD51, the complete assembly remained possible. The other three datasets (represented by the darker yellow curves) were obtained at pH 7.5. The curves in **b)** and **c)** were generated in the same way as in Supplementary Figure 7b,c. At pH 7.5, the values of the torque plateaus at negative and positive turns are −12 ± 5 and 32 ± 7 pN·nm, respectively. The difference in torque between the two plateaus is 44 ± 3 pN·nm, which agrees well with the results obtained in buffers containing Ca^{2+}-ATP or Ca^{2+}-AMPPNP. At pH 6.2, the values of the torque plateaus at negative and positive turns are −13 ± 7 and 17 ± 7 pN·nm, respectively, and the difference between them equals 30 ± 2 pN·nm. We note the value of the torque plateau at positive turns that we obtain at pH 6.2 is quite a bit lower than the corresponding value at pH 7.5. Possibly, a different mechanism could be involved in relieving torsional strain upon over-winding under these conditions. Dissociation of RAD51 monomers due to decreased binding affinity at lower pH could be a possible explanation; however, hysteresis indicative of protein dissociation was not observed in repeated measurements of rotation-extension curves. The bending and torsional persistence lengths were, within experimental error, independent of pH. By analyzing the datasets at pH 6.2 and 7.5 together, we obtained a torsional persistence length (C) of 273 ± 35 nm (mean and SEM for 6 measurements).